Submitted to the International Europhysics Conference on High Energy Physics, HEP97, Jerusalem, Israel, August 1997

A Measurement of the Inclusive Deep Inelastic *ep* Scattering Cross Section at Low Q^2 at HERA

H1 Collaboration

Abstract:

A new measurement of the proton structure function $F_2(x, Q^2)$ is reported for momentum transfers squared $2 < Q^2 < 90$ GeV^2 and for Bjorken-x values $10^{-5} < x < 0.1$ using data collected by the HERA experiment H1 in 1995 and 1996. A QCD analysis of this data combined with measurements of the structure function $F_2(x, Q^2)$ from earlier H1 measurements and fixed target experiments is presented. A new result on the longitudinal proton structure function $F_L(x, Q^2)$ for $12 < Q^2 < 35$ GeV^2 is extracted from the measurement of the ep differential cross-section in a kinematic range extended to large inelasticity values of y up to 0.86.

Abstract 260
Parallel Sessions 3,4
Plenary Sessions PL 1,3

1 Introduction

The measurement of the deep inelastic scattering (DIS) cross section, $\sigma(ep \to eX)$, has been one of the most important goals of the H1 experiment at HERA since its advent in 1992. In a series of measurements a number of interesting observations has been made:

- The structure function $F_2(x, Q^2)$ rises towards low x for Bjorken $x < 10^{-2}$ [1–3].
- The Q^2 behaviour has been successfully described by QCD evolution equations in NLO which leads to a large gluon distribution at low x [3].
- A measurement of the DIS cross section at high inelasticity values $y \leq 0.78$ was used to determine the longitudinal structure function $F_L(x, Q^2)$ [4].
- For very low four-momentum transfers squared $Q^2 < 1$ GeV^2 the rise of F_2 diminishes and approaches that expected in Regge and Vector Dominance Model interpretations [5].
- Very recently it was demonstrated that the behaviour of F_2 up to large $Q^2 \leq 5000$ GeV^2 and $x < 0.4$ is in accord with perturbative QCD within the measurement accuracy of about 10% [6].

Similar results have been obtained by the ZEUS experiment [7,8]. After these exploratory measurements of the DIS cross section at HERA, we are now entering a new phase of experimentation where precision and maximum coverage of the kinematic range are necessary in order to better understand the strong interaction dynamics.

This paper presents new, preliminary results from the analysis of cross section data taken in the years 1995 and 1996. For low Q^2, low x physics, which is measured with the backward part of the H1 detector, the backward proportional chamber and the electromagnetic Lead-scintillator calorimeter were replaced by a drift chamber (BDC) and a Lead-fibre calorimeter (SPACAL) [9], respectively. The following goals were set for the analysis described subsequently:

- An improved measurement of F_2 in the range $1 < Q^2 < 10$ GeV^2. This has been obtained with 0.6 pb^{-1} of data taken in 1995.
- A new measurement of F_2 for $10 < Q^2 < 100$ GeV^2 in order to complement the so far most precise H1 structure function data [3]. This has been done using 4.8 pb^{-1} of data taken in 1996.
- An improved determination of the gluon distribution for low $x \leq 10^{-2}$ using the QCD evolution equations.
- An extension of the kinematic range up to $y = 0.86$, i.e. down to energies of the scattered positron of 4 GeV, in order to enhance the sensitivity to F_L.

While the measurements of F_2 follow rather closely the previous H1 determinations, and are thus only briefly described here, rather novel techniques had to be developed in order to measure the DIS cross section down to positron energies of a few GeV only. These are presented here in more detail.

This paper is organized as follows. Section 2 summarizes the kinematic relations, information on the H1 experiment and describes the data taken in 1995 and 1996. Section 3 presents the new results on $F_2(x, Q^2)$ which are based on the cross section measurement up to $y = 0.7$. This data, combined with all previous H1 structure function results and also the proton and deuteron data of the NMC [10] and BCDMS [11] experiments, is used to perform a new NLO QCD fit which leads to an improved gluon determination as described in Section 4. In Section 5 the cross section measurement at very high y is discussed and a new result on the longitudinal structure function $F_L(x, Q^2)$ is deduced. A brief summary is given in Section 6.

2 Data

2.1 Kinematics

In 1995 and 1996 HERA was operated with protons of energy $E_p = 820$ GeV and positrons of energy $E_e = 27.52$ GeV and 27.57 GeV, respectively. The event kinematics were reconstructed using the energy of the scattered lepton E'_e and the polar angle θ_e according to the relations

$$y_e = 1 - \frac{E'_e}{E_e} \sin^2 \frac{\theta_e}{2} \qquad\qquad Q^2_e = 4E'_e E_e \cos^2 \frac{\theta_e}{2} = \frac{E'^2_e \sin^2 \theta_e}{1 - y_e}. \tag{1}$$

Here θ_e is defined with respect to the proton beam direction, defining the z axis. This reconstruction method, based on the scattered lepton, is called the 'electron (E)' method. It is best applicable at large values of y.

As in previous publications the Σ method is used to determine F_2 at low y. This method combines the positron and the hadronic measurements by defining

$$y_\Sigma = \frac{\Sigma}{\Sigma + E'_e(1 - \cos \theta_e)} \qquad\qquad Q^2_\Sigma = \frac{E'^2_e \sin^2 \theta_e}{1 - y_\Sigma}, \tag{2}$$

with

$$\Sigma = \sum_h (E_h - P_{z,h}) \tag{3}$$

and

$$y_h = \frac{\Sigma}{2E_e}. \tag{4}$$

Here E_h and $P_{z,h}$ are the energy and longitudinal momentum component of a particle h, the summation is over all hadronic final state particles, and masses are neglected. The denominator of y_Σ is equal to twice the energy of the true incident beam energy, which differs from the nominal beam energy if real photons are emitted by the incident positron. For both methods x is calculated as Q^2/sy with $s = 4E_pE_e$.

Another important quantity is the hadronic angle defined as

$$\tan\theta_h = \frac{\Sigma}{P_{t,h}} \tag{5}$$

where $P_{t,h}$ is the sum of transverse momenta of the hadronic final state particles. In the parton model θ_h defines the direction of the scattered quark. The scattering angles θ_e and θ_h are related according to

$$\tan\frac{\theta_h}{2} = \frac{y}{1-y} \cdot \tan\frac{\theta_e}{2}. \tag{6}$$

Thus for $y > 0.5$ the positron scattering angle θ_e is smaller than θ_h which was utilized for the positron identification at very small energies E'_e. Furthermore the two angles permit a positron energy calibration with an accuracy at the percent level in the kinematic peak region $E'_e \simeq E_e$.

2.2 The H1 Detector

The H1 detector [12] is a nearly 4π hermetic apparatus with a solenoidal magnetic field of 1.2 T built to investigate high-energy ep interactions at HERA. The scattered positron energy E'_e is measured in the backward electromagnetic Lead-fibre calorimeter (SPACAL) which has an integrated timing function to veto proton beam induced background interactions. Identification of the scattered positron and the polar angle measurement make use of a backward drift chamber (BDC) in front of the SPACAL. In the kinematic range of particularly low positron energies the positron angle θ_e is smaller than about 170^o, i.e. the positron traverses the inner cylindrical proportional chamber (CIP). In this energy region the inner and outer proportional chambers (CIP at 18 cm radius and COP at 47 cm radius) were used in the trigger to reduce beam induced background events. The interaction vertex was determined with the central drift chambers: the jet chamber CJC and the two z drift chambers. The hadronic final state was reconstructed with the Liquid Argon (LAr) calorimeter and the tracking detectors.

The luminosity was determined from the cross section of the elastic bremsstrahlung process, measured with a precision of 1.5% [13]. The final state photon and the positron scattered at very low Q^2 can be detected in calorimeters ("photon and electron taggers") which are situated close to the beam pipe at distances of 33 m and 103 m from the interaction point in the positron beam direction.

The use of the H1 detector for the inclusive DIS cross section measurement is further discussed in [3].

2.3 Data Selection

The data samples were collected with a minimum bias trigger requiring an energy deposit in the SPACAL to be above a certain threshold around 7 GeV. In the lower energy range the beam induced background is large and the SPACAL energy requirement had to be complemented by a track requirement using the multiwire proportional chambers. Because of occasionally high rates this trigger was prescaled by about a factor of 2.

	1995 (F_2)	1996 (F_2)	1996 (F_L)
luminosity [pb^{-1}]	0.615 ± 0.009	4.76 ± 0.07	2.62 ± 0.04
trigger thresholds	8 GeV	6.5 GeV	2 GeV
minimum E'_e	8 GeV	6.9 GeV	4 GeV

Table 1: *Summary of data samples used in this analysis. The data for $y < 0.7$ where used for a measurement of F_2. At very large y the cross section is rather sensitive to F_L and the data analysis which required partially different techniques has been labeled correspondingly.*

A strict data selection was applied requiring stable beam conditions and all important detector parts to be on. Detailed studies were made of the yield and the time stability of the data. Table 1 summarizes the main characteristics of the 1995 and the 1996 data samples used in this analysis.

2.4 Event Selection

The event selection criteria are summarized in table 2. The positron was identified as the most energetic cluster in the SPACAL, for the 1995 data, and the cluster with maximum transverse momentum p_t for the 1996 data. Since in neutral current events the p_t is balanced the positron for most of the events has the largest p_t, see sect.5.1. The SPACAL cluster had to be associated with a signal in the preceeding drift chamber (BDC) and, if geometrically available, with a signal in the CIP or a pointing track segment in the central drift chamber CJC. For the determination of the event kinematics and background suppression a vertex had to be reconstructed in the CJC. In the 1995 analysis a vertex was also accepted if reconstructed with the Forward Tracker.

The distributions of selected events were compared with simulations. Deep inelastic events were generated using the DJANGO [14] event generator. This program is based on HERACLES [15] for the electroweak interaction and on LEPTO [16] to simulate the hadronic final state. The DIS cross section was simulated using a recent parametrization of the parton distributions [17] and setting $F_L = 0$. A reweighting procedure was applied using the H1 QCD fit [3] and calculating F_L to NLO according to [18] for three light flavours and according to [19] for the charm contribution. Photoproduction background events were generated with the PHOJET [20] program. The detector response was simulated using a program based on GEANT [21]. The simulated Monte Carlo events were reconstructed and analyzed using the same program chain as for the real data. For comparisons with experimental distributions the simulated spectra have been normalized to the measured luminosity.

Detailed studies were performed of the detector alignment, of the cut efficiencies and of the resolution of the kinematic variables. Good agreement at the few percent level was reached between experiment and simulation for the large set of technical and physics distributions studied. For example, Figure 1 shows three distributions for the 1995 data sample compared with the Monte Carlo event simulation. The experimental energy, Q^2 and $E - p_z$ distributions agree well with the sum of the DIS event simulation and of the simulated photoproduction events (hatched in Figure 1). A similar set of reference distributions for the 1996 data sample ($y < 0.7$) is shown in Figure 2. The distributions are well described in shape and normalization by the simulation. The y_h distribution is well reproduced down to $y_h = 0.001$. The use of the data for $y_h < 0.01$, however, needs further studies due to resolution and calorimeter noise problems.

	1995 (F_2)	1996 (F_2)	1996 (F_L)
y range	0.01 - 0.7	0.01 - 0.7	0.7-0.85
Q^2 range [GeV^2]	2-8.5	12-90	12-35
z vertex position [cm]	$\|z\| < 30$	$\|z\| < 24$	$\|z\| < 24$
SPACAL cluster radius [cm]	ECRA < 3.5	RCLL < 4	RCLL < 4
SPACAL-BDC matching [cm]	$\delta r < 2$, $r\delta\phi < 2.5$	$\delta r < 2$, $r\delta\phi < 2.5$	$\delta < 3$
hadronic SPACAL energy	< 0.5 GeV	< 0.5 GeV	$< 15\%$ of E'_e
total $E - p_z$	> 35 GeV	> 35 GeV	> 35 GeV
validation with CIP	–	for $y > 0.6$	yes
CJC track radius	–	–	> 30 cm
SPACAL-CJC matching	–	–	< 6 cm
track charge	–	–	> 0

Table 2: *Basic event selection criteria. The 1995 analysis is very similar to the one described in [5] which was restricted to the 1995 data sample with the interaction vertex shifted in proton beam direction to access the very low Q^2 region. For the analysis of the 1996 data the cluster radius definition was changed from a mean radius (ECRA), calculated as the sum over the cell radii with energy weights $w_i = E_i$, to a mean (RCLL) using the expression $w_i = max(0, w_0 + ln(E_i/E_{tot})$ with $w_0 = 4.85$ [9]. The high y cross section analysis used tracks reconstructed in the CJC for positron identification and background suppression, see section 5.*

3 The Proton Structure Function $F_2(x, Q^2)$

The DIS cross section in the one-photon exchange approximation

$$\frac{\mathrm{d}\sigma}{\mathrm{d}x dQ^2} = \frac{2\pi\alpha^2}{Q^4 x} \cdot [(1 + (1-y)^2) F_2(x, Q^2) - y^2 F_L(x, Q^2)] = \kappa[F_2 - F_L \cdot \frac{y^2}{Y_+}] \tag{7}$$

depends on the two structure functions F_2 and F_L. Here Y_+ is equal to $1 + (1-y)^2$. Since there is the constraint $0 \leq F_L \leq F_2$, due to the positivity of the cross sections for longitudinal and transverse polarized photon scattering off protons, the measurement of $\mathrm{d}\sigma/\mathrm{d}xdQ^2$ is equivalent to a measurement of F_2 in almost the complete kinematic region. The H1 F_2 data are restricted to a range of Q^2 and x values with $y = Q^2/sx \leq 0.7$.

The cross section is determined by converting the measured number of events, after background subtraction, in a bin averaged cross section using acceptance calculations from the Monte Carlo sample. The data are binned in a grid in x and Q^2 as chosen previously [3]. All detector efficiencies were determined from the data using the redundancy of the apparatus. The bin averaged cross section is corrected for first order radiative contributions with the program HERACLES [15]. The radiative corrections, in particular for the E method at large y, are large and were calculated also with the HECTOR program [23]. Good agreement at the level of 1% was reached between these calculations. A bin size correction was performed to obtain the differential cross section. The F_2 data at large $y > 0.15$ are due to the E method and due to the Σ method for smaller y. In the region of overlap, $0.6 \leq y \leq 0.05$, the results from the two methods agree very well which is another indication for the correct treatment of the radiative corrections and also for a reliable energy calibration. All structure function data presented below were obtained in two independent analysis chains which analyzed all data, efficiencies and cross sections using both the E and the Σ methods.

source	effect on cross section [%]
positron identification	1-3
vertex efficiency	2
BDC efficiency	2
trigger efficiency	1
photoproduction background	max 5% at high y
radiative corrections	2
	calibration [%]
positron energy uncertainty	1-3
θ_e error in mrad	0.5-1
hadronic energy scale LAr/SPACAL	4/7

Table 3: *Sources of systematic errors and their effect on the cross section measurement accuracy and calibration uncertainty of the energy and angle measurements, respectively, quoted for the F_2 structure function analyses, $y < 0.7$. The resulting systematic errors for the E method ($y > 0.15$) and the Σ method are of comparable size ranging between 6% and 12% at the edges of the covered range. The systematic error is not dominated by a single source.*

Figure 3 presents the new data together with the previous structure function measurements of H1 and the higher x data of NMC. The 1995 data (full triangles) are the most precise F_2 data obtained by H1 so far in the Q^2 region between 2 and 8.5 GeV^2 [24]. The precision of this data is governed by systematic effects which amount to about 8-12%. The 1996 data [25] cover the larger Q^2 region between 12 and 90 GeV^2, closed circles in Figure 3. This data has an accuracy of about 6-10%. The systematic error sources are summarized in Table 3. There is remarkable agreement with the 1994 data although that was taken with a different apparatus in backward direction. Small departures between the two data sets are due to local systematic effects but are covered by the systematic errors assigned. The curves in Figure 3 represent a QCD fit to next-to-leading order which is used for a new determination of xg as described below.

The striking rise of F_2 towards low x has been quantified by determining the exponent λ of $F_2 \propto x^{-\lambda}$ at fixed Q^2. Figure 4 represents a preliminary update of our previous result [3,5] on the λ exponent including the recent H1 data on F_2 for $Q^2 > 100$ GeV^2 [6]. There is a smooth transition visible from large values of $\lambda \simeq 0.40$ for $Q^2 = 1000$ GeV^2 down to $\lambda \simeq 0.15$ for $Q^2 = 1$ GeV^2.

4 The Gluon Distribution $xg(x, Q^2)$

The gluon distribution can be extracted from the scaling violations of the structure function F_2. A NLO QCD fit was performed in the $\overline{MS}$ renormalization scheme using the DGLAP evolution equations [26] for three light flavours with the charm contribution added using the NLO calculation of the photon-gluon fusion process [17, 19]. The numerical solution of the DGLAP equations used the procedure described in [22]. The input parton distributions at the starting scale Q_o^2 were parametrized as follows:

$$
\begin{aligned}
xg(x) &= A_g x^{B_g}(1-x)^{C_g}, \\
xu_v(x) &= A_u x^{B_u}(1-x)^{C_u}(1+D_u x+E_u\sqrt{x}), \\
xd_v(x) &= A_d x^{B_d}(1-x)^{C_d}(1+D_d x+E_d\sqrt{x}), \\
xS(x) &= A_S x^{B_S}(1-x)^{C_S}(1+D_S x+E_S\sqrt{x}),
\end{aligned} \tag{8}
$$

where $S = \bar{u} = \bar{d} = 2\bar{s}$ defines the sea distributions. This analysis had the goal of determining the gluon distribution at low $x \leq 0.01$ where the bulk of the H1 structure function data is concentrated. The fit used this new data set and all published F_2 data from H1. In order to reduce the influence of the longitudinal structure function on this fit a cut of $y < 0.6$ was used for all H1 data sets. The minimum y is approximately equal to 0.01 for all Q^2 values. Besides the H1 data the proton and deuterium data of the muon scattering experiments BCDMS [11] and NMC [10] were used to constrain the high x behaviour of the parton distributions.

The starting point of the evolution was chosen to be $Q_o^2 = 1$ GeV^2 and all data with $Q^2 \geq 1.5$ GeV^2 were included in the fit. To avoid possible higher twist effects, data in the range $x > 0.5$ for $Q^2 < 15$ GeV^2 were not included in the fit. The normalizations of all data were allowed to vary taking into account the quoted luminosity errors. For the fit a value of $\alpha_s(M_Z^2) = 0.118$ was chosen. This fit is in very good agreement with the F_2 structure function measurement, see Figure 3.

The resulting gluon distribution is shown in Figure 5 for $Q^2 = 5$ and 20 GeV^2. The gluon distribution is rising towards low x. This is mainly due to the asymptotic behaviour in ln $1/x$ of the solutions to the DGLAP equations. The starting distribution $xg(x, Q_o^2)$ is found to have a valence shape falling steeply at low x. Several studies were made in order to understand the behaviour of this gluon determination [29]:

- The dependence of the resulting xg was studied on the starting scale Q_o^2. With a five parameter ansatz for $xg(x, Q_o^2)$ insensitivity is reached at the percent level against variations of Q_o^2 between 1 and 5 GeV^2. A low $Q_o^2 = 1$ GeV^2 was chosen since in this case three parameters only have to be introduced, the parameters D_g and E_g, see eq.8, not being required by the fit.

- The width of the error band of xg crucially depends on the size and treatment of the systematic errors. The procedure applied distinguished between random and correlated errors. In the calculation of the uncertainty of xg all point-to-point correlations between the data points were separately considered. The resulting xg band represents the error contour due to moving the individual F_2 sets separately according to the different error contributions. This procedure is equivalent to a method where the systematic errors are propagated to the covariance matrix of the fitted parameters as described in [27]. The new F_2 data presented here lead to an improvement of the xg determination by a factor of about 2. The width of the error band shown in Figure 5 takes into account a possible variation of α_s by ± 0.005 and of the charm quark mass m_c by ± 0.3 GeV.

- It is known that the determination of the gluon distribution using only charged lepton structure function data leads to a behaviour of xg at high x which differs from the results of global analyses which include direct photon data [28]. Therefore the result in Figure 5 is given only for $x < 0.01$. Moreover, a control fit was done with a five parameter gluon distribution fixing the parameters which determine the high x behaviour of xg in order to reproduce the high x gluon of [30]. This leads to a gluon distribution which is lower by nearly 10% at $x = 0.01$ but in very good agreement with the standard three parameter gluon at lower x. The difference of these two determinations has been included in the error band drawn in Figure 5. It is largely responsible for the error of xg at x near to 0.01.

5 Measurement of the Cross Section at Very Large y

5.1 Positron Identification and Photoproduction Background

The cross section measurement at y near to 1 is a particular challenge at HERA since it requires a positron identification in the region of energies of a few GeV. As explained above at these low energies the trigger requirement of energy deposited in SPACAL had to be complemented by a track requirement in order to get rid of beam induced background. Moreover, at low energies, even for $Q^2 \simeq 10$ GeV^2, the positron is scattered to rather low angles, i.e. $\theta_e \simeq 160^o$. Therefore in the H1 detector for largest y one can recognize the positron as a track in the CJC. This permits the subtraction of the photoproduction background using the charge assignment of these tracks. Since at low energies the positron has less energy than the hadronic final state which is also scattered backwards, the positron identification procedure had to be changed. Thus the unique features of the high y analysis are a modified positron identification and the requirement of a track with correct charge pointing to the SPACAL cluster, see Table 2.

Figure 6 shows a calculation of the efficiency to identify the true scattered positron with the standard selection criteria, i.e. without using the track requirement. The open points correspond to a selection of the maximum energy cluster which at low energies yields only 70% efficiency. A higher efficiency is achieved selecting the cluster with maximum transverse momentum, closed points. This efficiency depends obviously on the hadronic final state. Thus a comparison was made using different models, i.e. LEPTO [16] using the colour dipole model as implemented in ARIADNE [31], LEPTO with matrix element and parton shower generation and the HERWIG cluster fragmentation model [32]. Between these three models agreement was found within 2% for the maximum p_t requirement and 4% for the highest energy condition. From these Monte Carlo studies, extended also to a selection of clusters with minimum angle, and from the description of the next-to-leading cluster distributions, a positron identification error of 3% was derived. Although this analysis was extended to 3 GeV minimum energy for part of the data, for technical reasons a cut had to be set at 4 GeV.

Figure 7 shows a set of control distributions for the high y data analysis. The charge was reconstructed using the track curvature determined in the CJC. This determination was controlled by considering the azimuthal angle difference $\Delta\phi$ between the track angle at the interaction point, reconstructed in the CJC, and the straight line given by the vertex and the SPACAL cluster position. The sign of $\Delta\phi$ measures the direction of the track rotation and thus determines the charge of the particle independently of the track curvature measurement in the jet chamber. Figure 7a shows the $\Delta\phi$ distribution for selected candidate tracks with positive charge determined in the CJC track reconstruction (closed points). It is well described by the Monte Carlo simulation (open histogram). The dashed histogram represents the tracks with negative charge which have a different sign of $\Delta\phi$. For 99.5% of the tracks the charge assignment with the CJC and with $\Delta\phi$ agrees. The residual 0.5% can be explained by the tail of the SPACAL cluster ϕ distribution. Finally the CJC measurement of the track momentum (p) was cross checked with the SPACAL energy measurement (E) with a an energy dependent resolution of the E/p ratio of roughly 20% in good agreement with the simulation result.

A charge subtraction procedure could be applied because the photoproduction background was found to be charge symmetric. A direct experimental check comes from those events which have a tagged low Q^2 positron downstream the positron beam. Figure 7b shows the SPACAL energy spectrum of the positron candidates of those tagged events which obey the standard selection cuts, without the $E-p_z$ condition. The data were corrected for the tagger acceptance. Within the limited statistics the positive (closed points) and the negative (open points) background energy distributions are equal corresponding to at most 3% asymmetry of the integrated distributions. Moreover there is very good agreement with the SPACAL energy distribution for clusters linked to tracks with negative charge (histogram in Figure 7b). In a PHOJET study of the photoproduction background a limit was set of 1% residual charge asymmetry the error being due to the limited statistics simulated.

Figure 7c shows the SPACAL energy distribution of the positive candidates before charge subtraction. The experimental distribution is well described by the Monte Carlo simulation. Figure 7d shows the distribution of the scattering angle θ_e for energies < 7 GeV which as well is in good agreement with the sum of the DIS simulated spectrum and the negative charge distribution. Note that the cross section in the Monte Carlo simulation in this y range has been reweighted using the measured DIS cross section. To summarize, using linked tracks the large photoproduction background at low energies can be eliminated by charge subtraction, the residual uncertainty being due to the still limited statistics in data and simulation. The usage of tracks introduces another 3% systematic error due to the efficiency to link tracks to SPACAL clusters.

5.2 Cross Section Measurement

The result on the measured DIS cross section for Q^2 between 12 and 35 GeV^2 is shown in Figure 8 comparing the 1994 data [4] (open points) with this analysis of the 1996 data (closed points). The error bars comprise both statistical and systematic errors added in quadrature. Both cross section measurements agree well. For four Q^2 points the y range was extended to a mean $y = 0.82$ which considerably enhances the sensitivity to F_L. For $y = 0.68$ two methods could be employed either using tracks and charge subtraction of the background, as for $y = 0.82$, or following the standard treatment of the photoproduction background for lower y. These two cross section measurements agreed within 2% accuracy.

At large y the radiative corrections are large, of the order of 50%. Agreement was found between the HERACLES code and the HECTOR program to better than 2%. The effect of these corrections is reduced by an order of magnitude with the $E - p_z$ cut. A 3% error was assigned for the cross section error due to radiative corrections at these large y values. The acceptance calculation for the cross section measurement at high y was performed with the same input structure functions as the F_2 data analysis, i.e. using the previous H1 QCD fit [3] and its NLO prediction for F_L.

source	effect on cross section [%]
trigger efficiency	3
vertex efficiency	2
positron identification	3
photoproduction background	1
charge determination	1
track-cluster link efficiency	3
radiative corrections	3

Table 4: *Systematic errors of the cross section measurement for $y > 0.7$. In addition there are contributions due to the energy and angle calibration uncertainties as listed in Table 3.*

The systematic errors in addition to the calibration errors as given in Table 3 are summarized in Table 4. The total systematic cross section error at largest y is 8%, rather independently of Q^2 since most of the systematics at high y is dependent on the positron energy.

Figure 8 shows also calculations of the cross section using the QCD fit to F_2, described in Section 4, and three different assumptions on the longitudinal structure function F_L. The measured cross section is in agreement with the NLO QCD calculation apart from large y , for $12 \le Q^2 \le 25$ GeV^2, where the measured points tend to be lower than the QCD curves (solid curves in Figure 8).

5.3 Determination of $F_L(x, Q^2)$

The cross section measurement at high y [25] can be converted to a determination of the longitudinal structure function $F_L(x, Q^2)$ assuming that F_2 in this region is given by the DGLAP equations in NLO using the H1 and fixed target data as was discussed in [4]. In order to represent the cross section measurement as a determination of F_L, a QCD fit to the new H1 data (1995, 1996), for $y < 0.35$, and to the BCDMS and NMC data was performed and F_2 in the high y region of the H1 data was calculated. The result agrees within 2% with the former calculation of F_2 [4] which used the 1994 H1 data and the BCDMS data. The resulting F_L values are shown in Figure 9. For $y = 0.68$ the new result is in good agreement with the 1994 data (open points). The region of $y > 0.78$, i.e. of lowest x at fixed Q^2, was not accessible prior to this analysis.

The total error of F_L comprises three different sources as discussed in [4]: i) the uncorrelated part of the systematic error of the high y cross section measurement; ii) the systematic error of the cross section correlated to the error of the input data to the QCD fit and iii) the error due to different assumptions inherent in the QCD fit. Improvement of the low Q^2 measurement accuracy with the 1995 data reduced the second contribution by a factor of 1.5. The error due to the fit assumptions includes also the effect of the imperfect description of the gluon distribution at large x values, see Section 4. Out of the three error contributions the genuine high y cross section uncertainty is the dominating one. The errors of F_L at $y = 0.82$ are smaller than the errors at lower y mainly due to the enhanced sensitivity to F_L being $\propto y^2$. For a reduction of the errors and possible biases due to the F_2 extrapolation it is essential to restrict this analysis to the use of consistent data in the whole y range in order to profit from error cancellations and not to depend on few percent normalization or shape differences, respectively.

The data are compared with the calculation of F_L in NLO QCD (shaded band in Figure 9) using the fit described and the prescription of [18] for three light flavours and of [19] for the charm contribution. This calculation agrees very well with the previous calculation, presented in [4], although it used different input distributions and programs. The experimental uncertainty of this calculation has improved to about 6%. Most of the data points are higher than the QCD expectation which is also visible in the cross section measurement at high y, Figure 8. A further reduction of the experimental errors is an obvious challenge.

6 Summary

Based on data taken in the years 1995 and 1996 a new measurement of the deep inelastic ep scattering cross section has been presented. This leads to new, preliminary data on the proton structure function $F_2(x,Q^2)$ for $2 \leq Q^2 \leq 8.5$ GeV^2 from the 1995 data with 0.62 pb^{-1} luminosity and for $12 \leq Q^2 \leq 90$ GeV^2 from the 1996 data with 4.8 pb^{-1} luminosity. With an accuracy of about 8-12% the lower Q^2 data are the most precise data obtained by H1 in this kinematic range so far. The larger Q^2 data are accurate to 6-10% and thus represent an important validation of the previous measurement [3], which was obtained with a different backward apparatus. All F_2 structure function data sets of H1, combined with data from the BCDMS and the NMC fixed target experiments, have been used to improve the determination of the gluon distribution at low $x \leq 0.01$.

The kinematic range has also been extended to maximum inelasticity values of $y = 0.86$ which permitted a new measurement of the DIS cross section in the region of enhanced sensitivity to the longitudinal structure function $F_L(x,Q^2)$. The cross sections measured at large y are somewhat below the QCD expectation based on a NLO analysis using the lower y H1 and fixed target data. This leads to values of the longitudinal structure function $F_L(x,Q^2)$ which are larger than expected assuming that F_2 is accurately determined by this QCD calculation.

Acknowledgements We are very grateful to the HERA machine group whose outstanding efforts made this experiment possible. We acknowledge the support of the DESY technical staff. We appreciate the substantial effort of the engineers and technicians who constructed and maintain the detector. We thank the funding agencies for financial support of this experiment. We wish to thank the DESY directorate for the support and hospitality extended to the non-DESY members of the collaboration.

References

[1] H1 Collaboration, I. Abt et al., Nucl.Phys. **B 407** (1993) 515.

[2] H1 Collaboration, T. Ahmed et al., Nucl.Phys. **B 439** (1995) 471.

[3] H1 Collaboration, S. Aid et al., Nucl. Phys. **B 470** (1996) 3.

[4] H1 Collaboration, C. Adloff et al., Phys. Lett. **B 393** (1997) 452.

[5] H1 Collaboration, C. Adloff et al., Nucl. Phys. **B 497** (1997) 3.

[6] H1 Collaboration, A Measurement of the Proton Structure Function $F_2(x, Q^2$ at High Q^2 at HERA, paper submitted to the International EPS Conference, Jerusalem 1997, August 1997.

[7] ZEUS Collaboration, M. Derrick et al., Z. Phys. **C 72** (1996) 399 and references cited therein.

[8] ZEUS Collaboration, J. Breitweg et al., DESY preprint 97-135(1997); ZEUS Collaboration, paper N-646, submitted to the International EPS Conference, Jerusalem 1997, August 1997.

[9] H1 SPACAL group, R. Appuhn et al., Nucl. Instr. and Meth. **A 386** (1997) 397.

[10] NMC Collaboration, M. Arneodo et al., Nucl. Phys. **B 483** (1997) 3.

[11] BCDMS Collaboration, A.C. Benvenuti et al., Phys. Lett. **B223** (1989)485;
CERN preprint CERN-EP/89-06.

[12] H1 Collab., I. Abt et al., Nucl. Instr. and Meth. **A386** (1997) 310 and **A386** (1997) 348.

[13] H1 Collaboration, "Luminosity Measurement in the H1 Experiment at HERA", paper submitted to the ICHEP 1996, pa 17-024, Warsaw (1996).

[14] G. A. Schuler and H. Spiesberger, Proceedings of the Workshop on HERA Physics, Vol 3, eds. W. Buchmüller and G. Ingelman, Hamburg, DESY (1992), p. 1419.

[15] A. Kwiatkowski, H. Spiesberger and H.-J. Möhring, Computer Phys. Comm. **69** (1992) 155.

[16] G. Ingelman, Proceedings of the Workshop on HERA Physics, Vol 3, eds. W. Buchmüller and G. Ingelman, Hamburg, DESY (1992), p. 1366.

[17] M. Glück, E.Reya and A.Vogt, Z. Phys. **C 67** (1995) 433.

[18] E.B. Zijlstra and W. van Neerven, Nucl. Phys. **B 383** (1992) 525;
S.A. Larin and J.A.M. Vermaseren, Z Phys. **C 57** (1993) 93.

[19] E. Laenen et al., Nucl. Phys. **B 392** (1993) 162.

[20] R. Engel and J. Ranft, Phys. Rev. **D 54** (1996) 4244.

[21] R. Brun et al., GEANT3 User's Guide, CERN-DD/EE 84-1, Geneva (1987).

[22] C. Pascaud and F. Zomer, LAL preprint LAL/94-42.

[23] A.Arbuzov et al., Comp.Phys.Comm. **94** (1996) 128.

[24] More details on the 1995 data analysis can be found in
L. Schoeffel, Thesis, University of Paris VI, 1997, to be submitted;
A. Meyer, Thesis, University of Hamburg, 1997, to be submitted.

[25] More details on the 1996 data analysis can be found in
A. Glazov, Thesis, Humboldt University, Berlin, 1997, to be submitted;

[26] Yu. L. Dokshitzer, Sov. Phys. JETP **46** (1977) 641;
V. N. Gribov and L.N. Lipatov, Sov. J. Nucl. Phys. **15** (1972) 438 and 675;
G. Altarelli and G. Parisi, Nucl. Phys. **B126** (1977) 298.

[27] C. Pascaud and F. Zomer, LAL preprint LAL/95-05.

[28] W. Vogelsang and A. Vogt, DESY preprint 95-096(1995).

[29] More details on this QCD analysis are discussed in
F. Lehner, Thesis, University of Hamburg, 1997, to be submitted.

[30] A.D. Martin, R.G. Roberts and W.J. Stirling, Phys. Lett. **B 387** (1996) 419.

[31] L. Lönnblad, Computer Phys. Comm. **71** (1992) 15.

[32] G. Marchesini, Computer Phys. Comm. **67** (1992) 465;
G. Marchesini et al., hep-ph 9607393(1996).

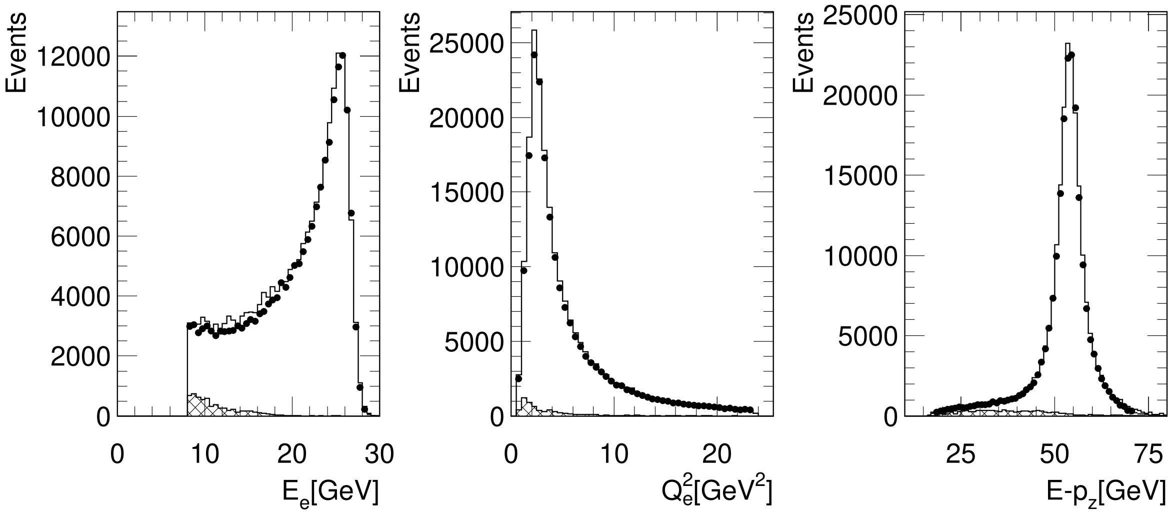

Figure 1: Distributions of the energy of the scattered positron, Q^2 and $E - p_z$ for the low Q^2 data sample taken in 1995. The histograms are a sum of the DIS event simulation and the simulated background from photoproduction (hatched). The simulated spectra are normalized to the luminosity of the data.

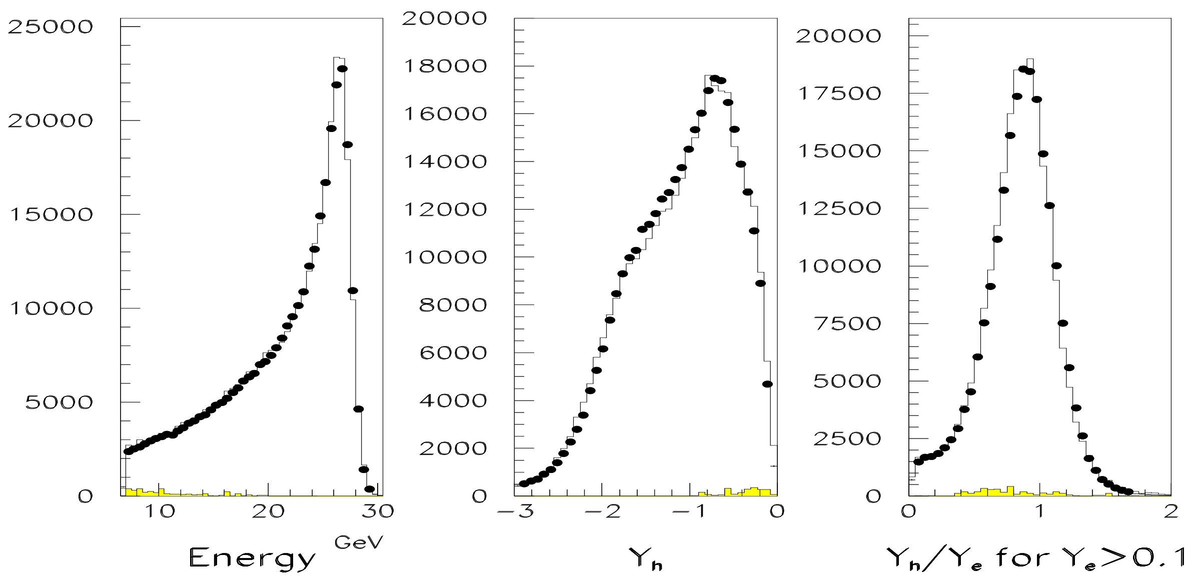

Figure 2: Distributions of the energy of the scattered positron, $\log_{10} y_h$ and the ratio y_h/y_e for the large Q^2 data sample taken in 1996. The histograms are a sum of the DIS event simulation and the simulated background from photoproduction (hatched). The simulated spectra are normalized to the luminosity of the data.

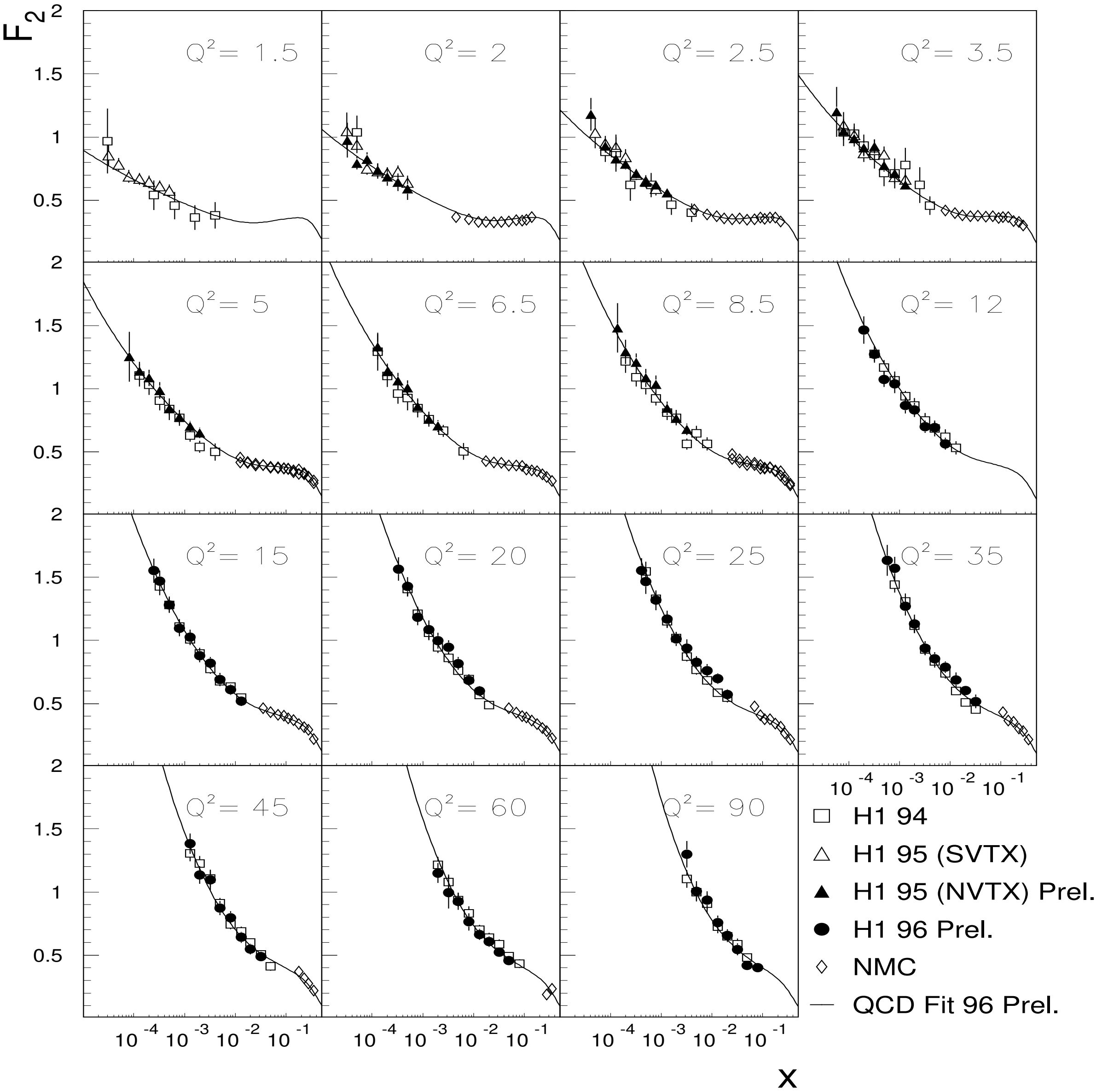

Figure 3: Measurements of F_2 by the H1 experiment. The new data (1995 data for Q^2 between 2 and 8.5 GeV^2 and 1996 data for Q^2 between 12 and 90 GeV^2) are in good agreement with the previous results on F_2 which used a different detector, apart from the 1995 shifted vertex data (SVTX). The curves represent the preliminary result of a NLO QCD fit to the H1, NMC and BCDMS structure function data, described in Section 4.

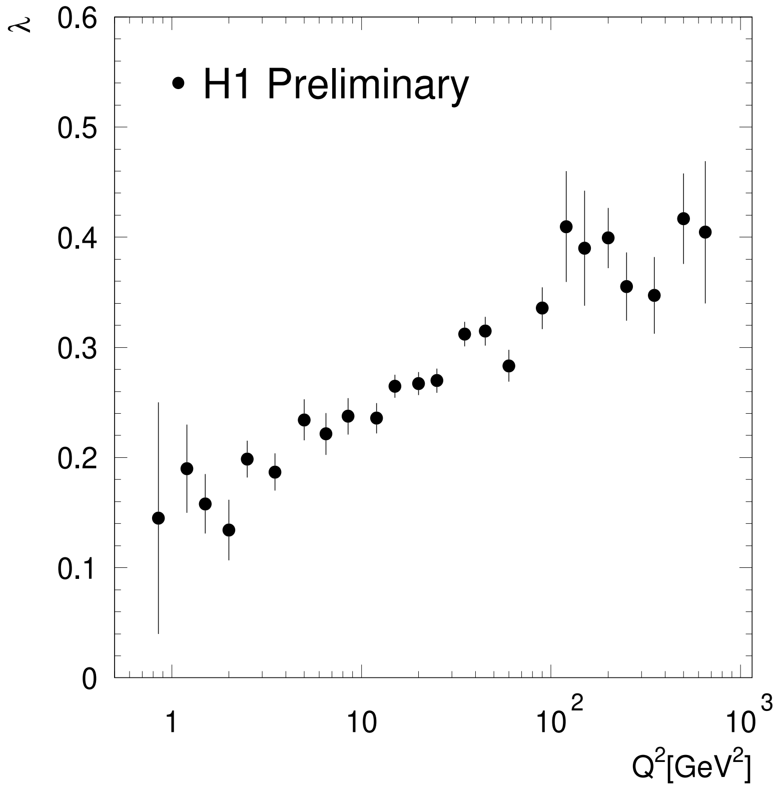

Figure 4: Derivative $\partial \ln F_2/\partial \ln(1/x)$ determined in each Q^2 bin from a straight line fit to $\ln F_2 = a + \lambda \cdot \ln(1/x)$. The fit uses all published H1 structure function data for $x > 0.1$. Note that there could be a hidden x dependence of λ since with rising Q^2 the mean x increases.

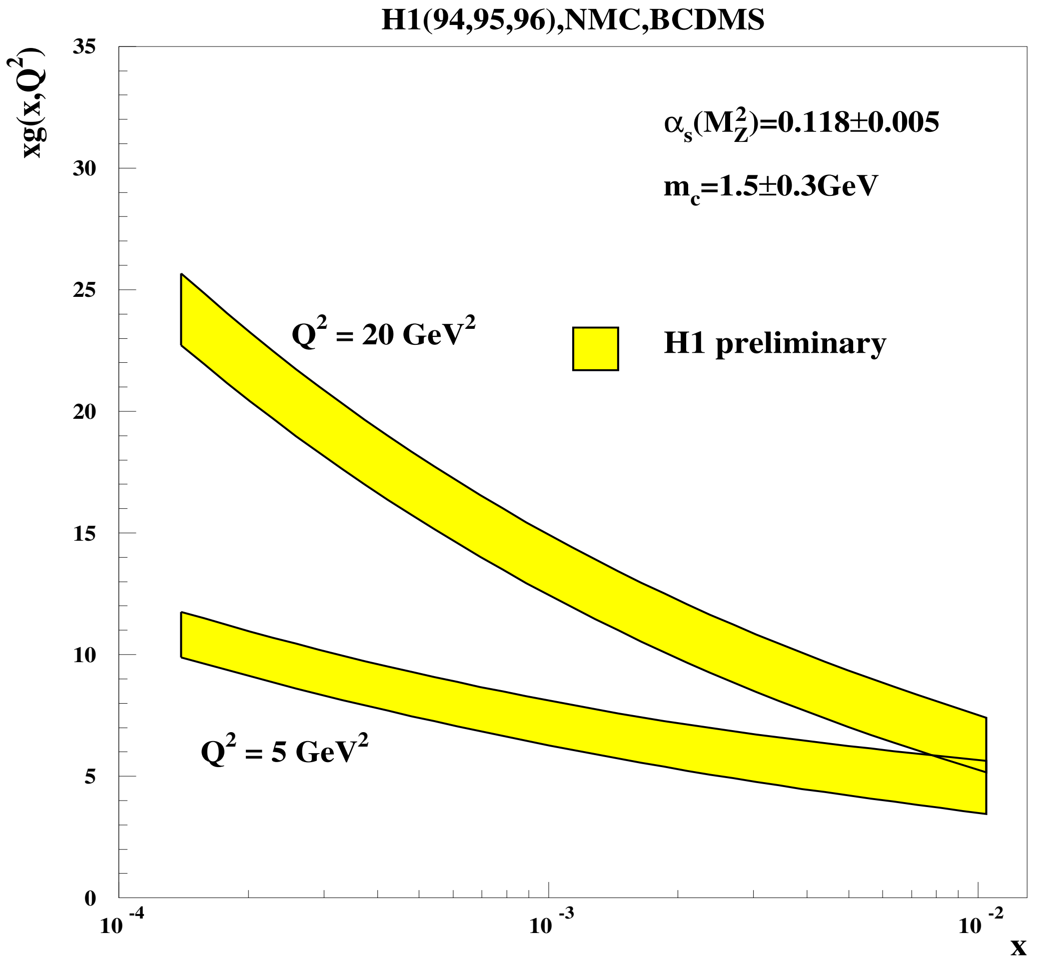

Figure 5: Gluon distribution resulting from a NLO QCD fit to all H1 structure function data (apart from the very recent high Q^2 data presented to this conference [6]), to the recent NMC and the BCDMS data. The error band comprises the statistical and systematic errors and also the uncertainties due to α_s, the charm quark mass m_c and due to the loosely constrained behaviour of xg at high $x > 0.1$. This result is compatible with but lower than the previously determined xg. Its validity is limited to the range $x < 0.01$ where the H1 data are concentrated.

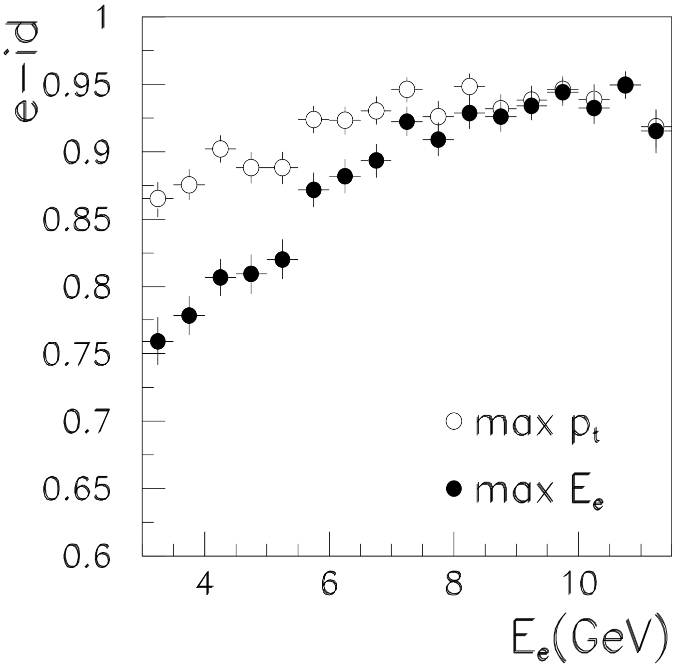

Figure 6: Calculation of the positron identification probability in the standard DIS event simulation requiring the scattered DIS positron to be either the cluster with maximum energy (closed points) or with maximum transverse momentum (open points). No track requirement is imposed.

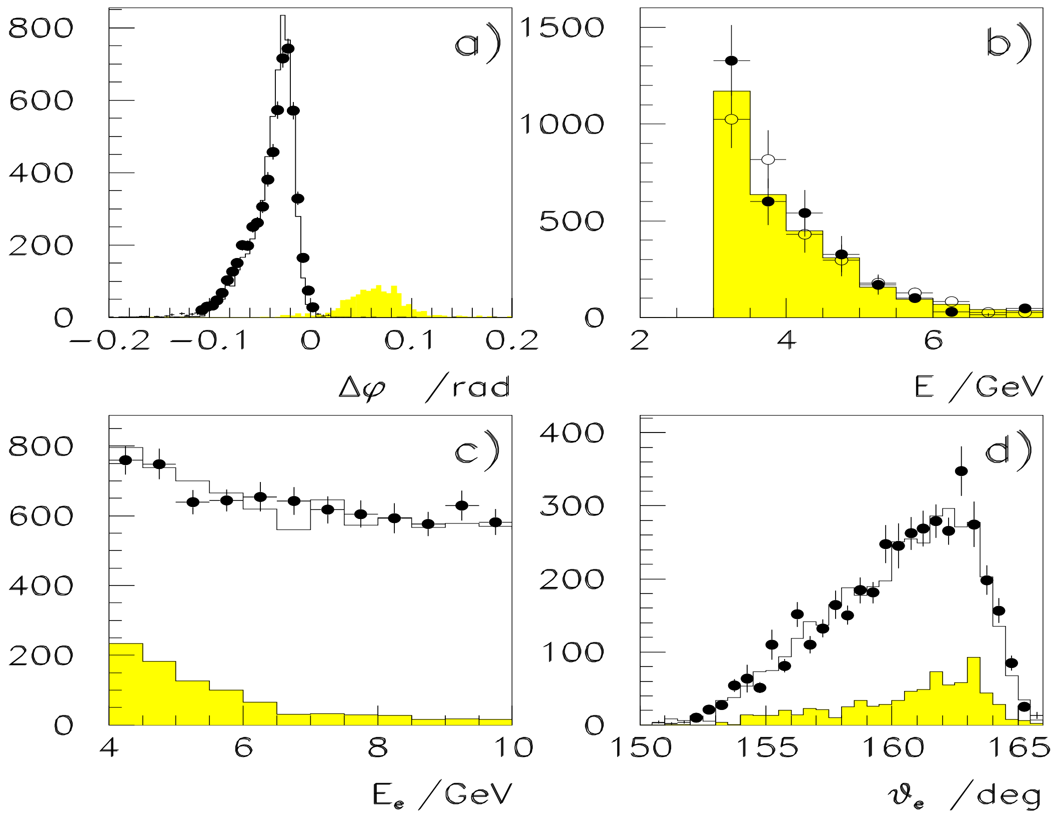

Figure 7: Distributions illustrating the cross section measurement at high y: a) difference $\Delta\phi$ of azimuthal angles determined from the jet chamber track and from a straight line connecting the interaction vertex position with the position of the SPACAL cluster for positron candidates with $3 < E'_e < 15$ GeV, closed points: data with positive track charge, open histogram: Monte Carlo simulation, shaded histogram: data with negative charge. b) SPACAL energy distributions before application of the $E - p_z$ cut, closed (open) points: tagged events with positive (negative) charge corrected for tagger acceptance, histogram: experimental SPACAL energy distribution for negative charge candidates. c) positron candidate energy distribution before charge subtraction for positive data (closed points), for negative data (shaded histogram) and for the sum of DIS Monte Carlo events and negative data (open histogram). d) polar angle distributions for positron candidates of energy between 4 and 7 GeV, same symbols used as in c).

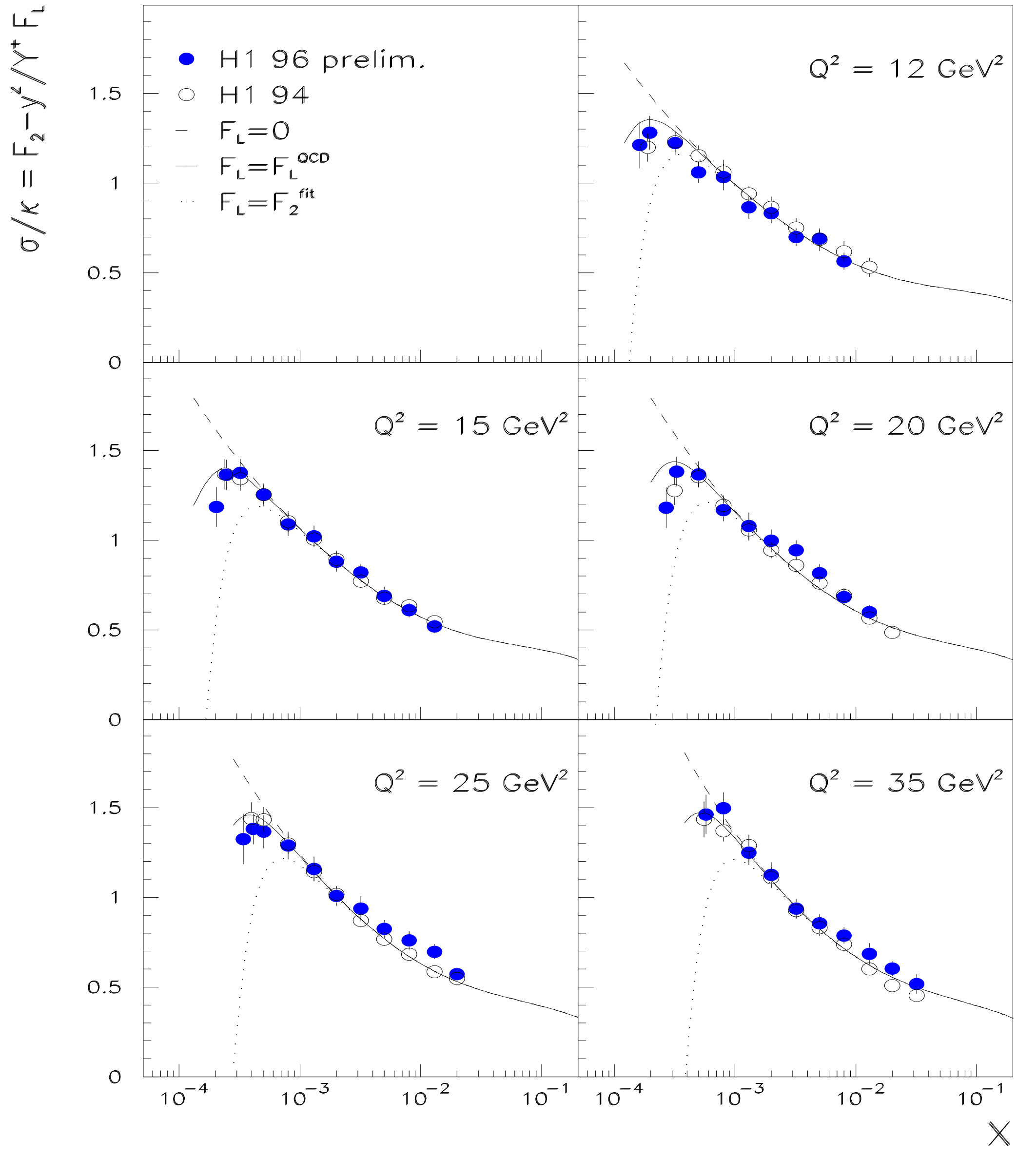

Figure 8: Measurement of the DIS cross section, eq.7, divided by the kinematic factor $\kappa = (2\pi\alpha^2 \cdot Y_+)/(Q^4 x)$. Closed points: this measurement, open points: H1 data from the 1994 run [4] taken with the former backward setup. The curves use the QCD calculation of F_2 and of F_L (closed curve) or the extreme assumptions $F_L = F_2$ (dotted curve) and $F_L = 0$ (dashed curve). The largest central y values are 0.82. For $Q^2 \geq 35$ GeV^2 this y range is outside the SPACAL acceptance.

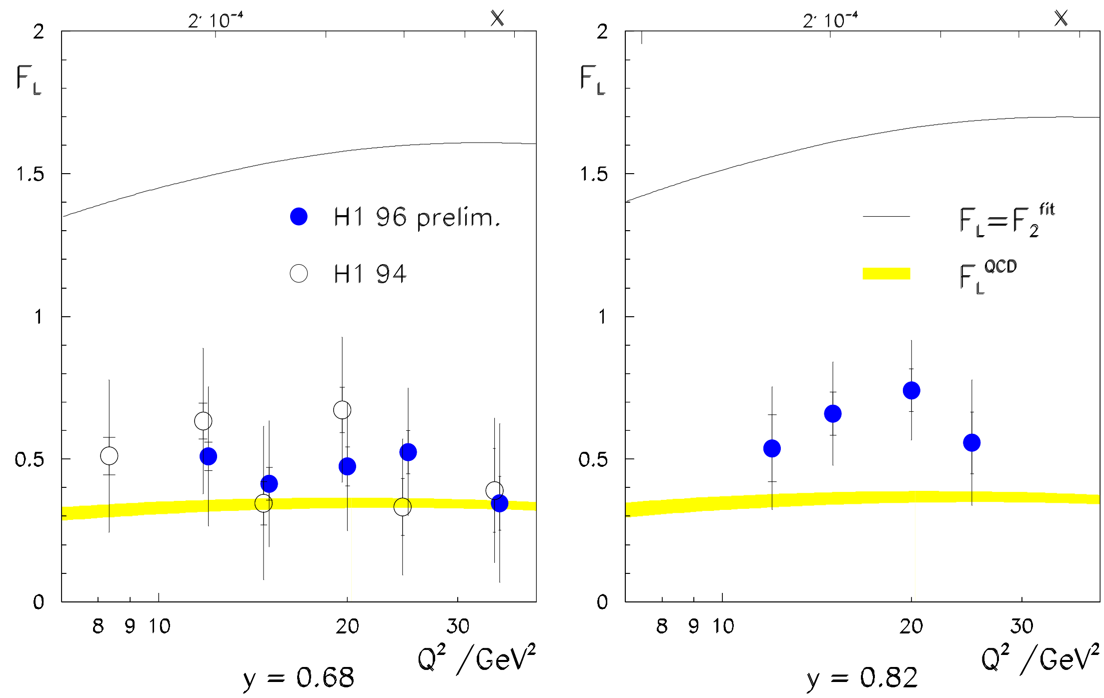

Figure 9: Longitudinal structure function $F_L = (F_2^{QCD} - \sigma/\kappa) \cdot Y_+/y^2$ determined as function of Q^2 or $x = Q^2/sy$ for $y = 0.68$ and $y = 0.82$. The closed points represent the preliminary result of this analysis while the open points are published H1 data [4]. The inner error bars are the statistical error. The full error bars represent the statistical and systematic errors added in quadrature. The error bands represent the uncertainty of the calculation of F_L using the gluon and quark distributions as determined from a NLO QCD analysis of the new H1 data for $y < 0.35$ and the fixed target experiment data. The upper line defines the allowed upper limit of $F_L = F_2$ where F_2 is given by the QCD fit.